Author Manuscript

Author Manuscript

Author Manuscript

Author Manuscript

HHS Public Access

Author manuscript

Neuroimage. Author manuscript; available in PMC 2017 February 01.

Published in final edited form as:

Neuroimage. 2016 February 1; 126: 72–80. doi:10.1016/j.neuroimage.2015.11.033.

Activity-induced manganese-dependent MRI (AIM-MRI) and functional MRI in awake rabbits during somatosensory stimulation

Matthew P. Schroeder[a], **Craig Weiss**[a], **Daniel Procissi**[b], **Lei Wang**[b,c,1], and **John F. Disterhoft**[a,*,1]

[a]Department of Physiology, Feinberg School of Medicine, Northwestern University, 303 E. Chicago Avenue, Ward Building 7-140, Chicago, IL 60611, USA

[b]Department of Radiology, Feinberg School of Medicine, Northwestern University, 737 North Michigan Avenue, Suite 1600, Chicago, IL 60611, USA

[c]Department of Psychiatry and Behavioral Sciences, Feinberg School of Medicine, Northwestern University, 710 N. Lake Shore Drive, Abbott Hall 1322, Chicago, IL 60611, USA

Abstract

Activity-induced manganese-dependent MRI (AIM-MRI) is a powerful tool to track system-wide neural activity using high resolution, quantitative T_1-weighted MRI in animal models and has significant advantages for investigating neural activity over other modalities including BOLD fMRI. With AIM-MRI, Mn^{2+} ions enter neurons via voltage-gated calcium channels preferentially active during the time of experimental exposure. A broad range of AIM-MRI studies using different species studying different phenomena have been performed, but few of these studies provide a systematic evaluation of the factors influencing the detection of Mn^{2+} such as dosage and the temporal characteristics of Mn^{2+} uptake.

We identified an optimal dose of Mn^{2+} (25 mg/kg, s.c.) in order to characterize the time-course of Mn^{2+} accumulation in active neural regions in the rabbit. T_1-weighted MRI and functional MRI were collected 0–3, 6–9, and 24–27 h post-Mn^{2+} injection while the vibrissae on the right side were vibrated. Significant BOLD activation in the left somatosensory (SS) cortex and left ventral posteromedial (VPM) thalamic nucleus was detected during whisker vibration. T_1-weighted signal intensities were extracted from these regions, their corresponding contralateral regions and the visual cortex (to serve as controls). A significant elevation in T_1-weighted signal intensity in the left SS cortex (relative to right)was evident 6–9 and 24–27 h post-Mn^{2+} injection while the left VPM thalamus showed a significant enhancement (relative to the right) only during the 24–27 h session. Visual cortex showed no hemispheric difference at any timepoint. Our results suggest that studies employing AIM-MRI would benefit by conducting experimental manipulations 6–24 h after subcutaneous $MnCl_2$ injections to optimize the concentration of contrast agent in the regions active during the exposure.

*Corresponding author at: 303 E. Chicago Ave., Ward 7-158, Chicago, IL 60611, USA.

[1]Contributed equally to this work.

Author Manuscript Author Manuscript Author Manuscript Author Manuscript

Keywords

Manganese-enhanced MRI; Functional magnetic resonance imaging; Activity-induced; Rabbit; Somatosensory; Awake animal MRI

Introduction

Magnetic resonance imaging (MRI) is a powerful tool to study neural processing in animal models but is limited by the types of experiments that can be performed. Anesthesia or sedation is often required in animal species undergoing MRI and while these pharmaceutical approaches maintain relative immobility and reduce MR signal artifacts, they can also alter the cognitive state of the animal and the physiology underlying hemodynamic correlates of neural activity (Brevard et al., 2003; Liu et al., 2013; Silva and Bock, 2008). In addition, the reduced brain size of most laboratory animals used in cognitive behavioral and neuroimaging studies presents additional technical challenges requiring high spatial and temporal resolution. As a result, MR techniques to study functional activation in animal models are limited.

Activity-induced manganese-dependent magnetic resonance imaging (AIM-MRI) is a technique to detect neural regions preferentially active during a task by using the paramagnetic MR contrast agent manganese (Mn^{2+}). Mn^{2+} can enter neurons during action potentials via active voltage-gated calcium (Ca^{2+}) channels (Aoki et al., 2002; Lin and Koretsky, 1997; Narita et al., 1990; Silva et al., 2004) in addition to other routes of Ca^{2+} and/or magnesium (Mg^{2+}) transport like sodium (Na^{+})/Ca^{2+} exchanger and the Na^{+}/Mg^{2+} antiporter (Crossgrove and Zheng, 2004). The more active a neuron is, the more Mn^{2+} will accumulate thereby producing a greater change in MR signal intensity (Lin and Koretsky, 1997). This is due to the fact that Mn^{2+} shortens the T_1-weighted (T_1W) and T_2-weighted (T_2W) relaxation times for water molecules in tissue as they realign to the static MR field after a disorienting gradient pulse (Inoue et al., 2011; Silva et al., 2004).

AIM-MRI also avoids interactions with cerebral blood flow and cerebral blood volume effects (Lee et al., 2010; Logothetis et al., 2001). Because Mn^{2+} acts as a calcium analog (Drapeau and Nachshen, 1984), AIM-MRI is more directly attributable to neuronal activation (Lev-Tov and O'Donovan, 1995; McClellan et al., 1994; Regehr and Tank, 1992; Yoshida et al., 2001) than is the blood-oxygen-level dependent (BOLD) response. Additionally, experimental manipulations in conjunction with AIM-MRI can either be performed inside or outside of the MRI environment using still or free-moving animals. Once inside a neuron, Mn^{2+} becomes temporarily sequestered (Watanabe et al., 2014) in the tissue by binding to proteins and nucleic acids (Silva, 2012) as opposed to some molecular storage site inaccessible to water (Chuang et al., 2009). From studies involving intracranial injections, Mn^{2+} is gradually transported to axon terminals in an anterograde fashion via fast axonal transport over the course of 24–48 h (Pautler et al., 1998; Sloot and Gramsbergen, 1994; Takeda et al., 1998; Tjälve et al., 1995; Watanabe et al., 2004) where it is then released into the synaptic cleft (Takeda et al., 1998). Hence, Mn^{2+} accumulation can be

Author Manuscript Author Manuscript Author Manuscript Author Manuscript

assessed via MRI at a later time representing a “snapshot” of the regions that were activated by the manipulation.

Studies employing Mn^{2+} vary in terms of dosages, injection methods, research objectives, and species (see Silva and Bock, 2008; Silva, 2012; Cacace et al., 2014 for a comprehensive review). In regard to AIM-MRI, a primary issue is when and how long experiments should be performed in relation to Mn^{2+} administration so that enough Mn^{2+} is available for uptake during the exposure. Some studies have been relatively brief. Berkowitz et al. (2006) injected rats intraperitoneally (i.p.) and placed separate groups in light or dark environments for 4 h before MR imaging to see T_1W enhancement in visual cortex. Weng et al. (2007) also injected rats i.p. and vibrated their whiskers for 3 consecutive hours prior to MR imaging to witness T_1W enhancement in somatosensory cortex. Other studies have tripled the exposure time to 9 h in order to compare groups exposed to light and dark environments (Bissig and Berkowitz, 2009). Others still have delivered stimuli for 24 h (Watanabe et al., 2008) and 48 h (Kimet al., 2014) to detect differences in T_1W enhancement after exposure to auditory stimuli. As can be seen, there is not a consensus regarding the optimal duration of experimental manipulation to see Mn^{2+} enhancement.

However, Mn^{2+} has some associated challenges. Subcutaneous injection of Mn^{2+} can result in skin irritation and lesions at the site of injection (Sepúlveda et al., 2012). Acute overexposure to Mn^{2+} can lead to cardiotoxicity (Wolf and Baum, 1983) and/or hepatic failure (Chandra and Shukla, 1976) after intravenous or intraperitoneal injection, respectively, due to inactivation of antioxidant enzymes, glutathione depletion and/or increased malondialdehyde in the liver (Bertin et al., 2010; Thuen et al., 2008). Often, studies temporarily and reversibly open the blood–brain barrier (BBB)with D-mannitol to quickly get a sufficient amount of Mn^{2+} into CSF so that it is available to active neural regions, although a number of studies have used Mn^{2+} without the need to disrupt the BBB (Berkowitz et al., 2006; Bissig and Berkowitz, 2009; Bock et al., 2008a; Kuo et al., 2006, 2007). In the absence of BBB disruption, the likely mechanism for Mn^{2+} transport into the brain is via a unidirectional blood-to-CSF transport (Bornhorst et al., 2012; Schmitt et al., 2011). Finally, the toxic effects of Mn^{2+} appear to be mediated by an animal's metabolic rate (Furchner et al., 1966). Dosages of Mn^{2+} need to be calibrated with careful attention to the species' physiology and metabolism to guarantee subject well-being. In rats, concentrations as high as 175 mg/kg have been injected intravenously (Bock et al., 2008b) and 300 mg/kg subcutaneously (Shazeeb and Sotak, 2012) although the majority of studies use a much lower systemic dose, inject in a fractionated manner (Bock et al., 2008b) or use an osmotic pump to ameliorate peripheral toxicity (Eschenko et al., 2010). To assess issues regarding different injection methods, Mn^{2+} concentration and efficacy, we conducted a pilot study with nine rabbits looking at four different protocols: intravenous, fractionated subcutaneous dosing over ten days, and two different concentrations injected as a subcutaneous bolus. We also collected blood samples to assess toxicity and MRI images to determine adequate signal enhancement.

Rabbits have advantages for AIM-MRI and the study of Mn^{2+} accumulation. In regard to MR imaging, a relatively simple surgery to implant atraumatic restraining bolts enables the rabbit to remain in a docile, awake state throughout scanning. The issues highlighted by

Author Manuscript Author Manuscript Author Manuscript Author Manuscript

Silva and Bock (2008) regarding anesthesia's deleterious effects on neural electrical activity are absent in the rabbit animal model since the rabbit can be imaged without the need for any sedation or anesthetic agents. Rabbits also have a lower mass-specific metabolism rate compared to rats or mice (Couture and Hulbert, 1995; Dobson and Headrick, 1995; Porter and Brand, 1995) thus minimizing the toxic effects of Mn^{2+}. These justifications make the rabbit an ideal animal model for AIM-MRI studies of which this is the first.

In this work, we collected T_1W high-resolution MRI and BOLD MRI in awake and conscious rabbits undergoing somatosensory stimulation of the right-sided whiskers during three sessions; 0–3, 6–9, and 24–27 h after subcutaneous administration of Mn^{2+}. Examining the left (activity-dependent) and right (non activity-dependent) hemispheres using BOLD imaging concurrently with AIM-MRI in awake animals not impaired by anesthesia provides a unique platform to investigate the underlying physiology of both techniques.

Methods

Subjects and surgical preparation for AIM-MRI experiments

Ten female, New Zealand White rabbits (mean weight = 3.78 kg (s.d. = 0.45)) were used for AIM-MRI experiments and nine rabbits (2–4 kg) were used to determine the safety of different doses (detailed in section Subjects used to determine safety and efficacy of Mn^{2+}). Surgery was performed under NIH and Northwestern University approved protocols to implant a custom-built restraining bolt assembly onto the rabbit's skull to be able to fix the head in a custom-built MR cradle. Anesthesia was induced with ketamine (60 mg/kg, i.m.) and xylazine (10 mg/kg, i.m.). Buprenex (0.03mg/kg, s.c.) was administered to minimize discomfort during and after the surgical procedure and ophthalmic ointment was applied to keep the eyes moist. After rabbits were placed into a stereotaxic apparatus, the scalp was incised and the skull was positioned with lambda 1.5 mm below bregma. In order to secure the headpost onto the skull, six holes (four rostral to bregma and two lateral to lambda) were drilled into (but not through) the skull. Nylon machine screws were turned into holes threaded with a 2–56 bottoming tap. Grip cement (Dentsply) was placed on the skull and machine screws and a custom-built headpost assembly (four upright nylon bolts (6–32 × 3/4″) encased in Grip cement) was lowered onto the cement-covered skull. Additional cement was added as necessary. Metacam (0.2 mg/kg, s.c.) was administered once the rabbits were sternal and 24 h later to provide analgesia.

Subjects used to determine safety and efficacy of Mn^{2+}

Nine female, New Zealand White rabbits (2–4 kg) were used to determine the safety of different doses of 1 M $MnCl_2$ (Sigma-Aldrich, St. Louis, MO, USA) made in 100 mM bicine buffer (pH = 7.4) (Seo et al., 2011). Rabbits were divided into four groups; 100 mg/kg delivered intravenously through the marginal ear vein (n=1), fractionated dosing of 5 mg/kg subcutaneous injections per day for 10 days (n=4), and 25 mg/kg (n= 2) and 50 mg/kg (n= 2) bolus injection of $MnCl_2$. Subcutaneous injections were distributed over four injection sites in the lumbar region.

Author Manuscript Author Manuscript Author Manuscript Author Manuscript

Blood samples were collected daily via the marginal ear vein in order to determine alterations on an eighteen panel screen. T_1W anatomical scans were acquired to determine alterations in signal intensity as a result of Mn^{2+} accumulation (individual scan time = 10 min, TR = 600 ms, TE = 2.09 ms, flip angle = 45°, 40 slices, 1.0 mm slice thickness, 0.5 × 0.5 mm in-plane resolution).

Animal restraint

One week after surgery, rabbits underwent a one-day habituation protocol to the MRI scanner environment. For habituation and all subsequent scanning, earplugs were inserted and rabbits were placed in a prone position inside a cotton wrap and a canvas bag (Lomir) secured with Velcro. A single-channel, receive only RF coil was secured to the underside of a Plexiglas crossbar which then was secured onto the rabbit's headpost with four nylon nuts. The crossbar and surface coil were fastened to the custom-built cradle to stabilize the rabbit's head and prevent movement. The cradle was placed in the MR scanner and the scanner ran a one hour EPI sequence to fulfill habituation training.

$MnCl_2$ administration and experimental setup

1 M $MnCl_2$ (25 mg/kg; Sigma-Aldrich, St. Louis, MO, USA) was diluted in 100 mM bicine buffer to produce solutions in a total volume of 40 mL with a pH level of 7.4 (Seo et al., 2011) (see discussion for rationale in using 25 mg/kg $MnCl_2$). Rabbits were administered 10 mL at each of four sites in the lumbar region; two bilateral injections caudal to the shoulder region and two bilateral injections ~2 inches more caudal to the first injections.

A 0.5″ × 3″ post-it note was attached to the rabbit's row B whiskers (on the right side) which was then attached to a fiber band within the MR cradle. A coil capable of inducing 60 Hz deflections of 150 μm was fastened to the fiber band thus making it possible to control whisker vibration from outside the scanner. For further details, see Li et al. (2012).

Experimental task design and MRI data acquisition

Rabbits underwent MR scanning in a Bruker 7 T/30 cm wide horizontal magnet (ClinScan, Bruker Biospin, Ettlingen, Germany) using the previously mentioned single-channel surface coil. Transmission was achieved with a two channel volume coil fixed inside the magnet. The following protocol (lasting ~3 h) was performed during imaging sessions that began 0, 6 and 24 h after the $MnCl_2$ injection to determine the time course of activity-dependent Mn^{2+} accumulation. Throughout each session, a block design was employed with 30 s sets of right whisker deflections of approximately 150 μm at 60 Hz followed by 30 s of no vibration. This relatively high vibration frequency was chosen based on successful whisker-signaled conditioning during delay and trace paradigms (Das et al., 2001; Galvez et al., 2006) and detection of significant BOLD signal changes in whisker cortex to 40 Hz vibration as reported in our previous work (Li et al., 2012).

To detect signal intensity changes as a result of Mn^{2+} accumulation, T_1W anatomical scans were acquired (individual scan time = 10 min, TR = 600 ms, TE = 2.09 ms, flip angle = 45°, 40 slices, 1.0 mm slice thickness, 0.5 × 0.5 mm in-plane resolution). To detect BOLD activation in response to whisker vibration, blood oxygen level-dependent (BOLD) contrast-

Author Manuscript Author Manuscript Author Manuscript Author Manuscript

sensitive T_2^*-weighted gradient-echo echo-planar images (EPIs) were acquired (individual scan time = 10 min, repetition time (TR) = 2.5 s, echo time (TE) = 25ms, flip angle = 90°, 20 coronal slices, 2.0 mm slice thickness, 0.5 × 0.5 mm in-plane resolution). MR scans (two anatomical, one BOLD scan) were acquired repeatedly producing a total of ten anatomical and five EPI scans for each session (Fig. 1). After each session, rabbits were returned to their home cage and kept under similar conditions. Sensitivity to touch at the injection sites and general temperament was assessed 4, 5, and 10 h after $MnCl_2$ injection. None of the rabbits exhibited sensitivity to touch and general temperament was good.

BOLD EPI processing and statistical analysis

Data analysis was performed with AFNI (Cox, 1996). The first four volumes of each functional dataset were discarded to reach saturation. Each EPI dataset was preprocessed with slice-timing correction, motion correction and spatial normalization. First-level analysis of the functional time series used a boxcar hemodynamic response function to model the stimuli of interest (i.e., duration of 30 s whisker vibration) to yield least squares estimates (i.e., percent BOLD signal change from baseline) and t-statistics of the linear regression coefficients. A repeated-measures ANOVA was performed to determine significant activation during whisker vibration across each of the three sessions. A minimum individual voxel threshold of $p < .001$ and minimum cluster size of ≥5 voxels was used to correct for multiple comparisons to produce a corrected p value of ≤.05. Post-hoc analyses were then performed on the regions showing significant activation and their corresponding counterpart in the contralateral hemisphere in addition to an ROI from the visual cortex (to serve as a control).

AIM-MRI processing and statistical analysis

In order to evaluate AIM-MRI effects associated with whisker vibration-induced activation, signal intensities from the T_1W anatomical scans were extracted from the regions showing significant BOLD activation in response to whisker vibration as determined above. Signal intensities from corresponding regions in the contralateral hemisphere and an ROI in the visual cortex were extracted to serve as control regions not expected to exhibit activity-dependent contrast changes. To understand the pharmacokinetics of Mn^{2+} in the rabbit, signal intensities from the cerebrospinal fluid and the whole brain were extracted. T_1W signal intensity for each timepoint was normalized (nSI) to the average signal intensity of the anterior and posterior pituitary gland (Pit) collected during the same timepoint to account for interscan and intersession variability. The Pit, which lacks a blood–brain barrier, reflects non-specific Mn^{2+}-related signal intensity changes not associated with neural activation (Chuang and Koretsky, 2009). nSI time courses were then scaled relative to the first acquired scan from the first post-Mn^{2+} injection session to determine percent change in nSI time courses. Linear mixed models (time within session, session, and hemisphere as fixed main effects) were used on these values to determine hemispheric differences in normalized T_1W signal intensity (presumably as a result of Mn^{2+} accumulation) across the three sessions (i.e., 0–3, 6–9, and 24–27 h after $MnCl_2$ injection). Post-hoc analyses determined whether a significant difference existed between hemispheres within each session.

Author Manuscript Author Manuscript Author Manuscript Author Manuscript

Tissue extraction and inductively coupled plasma mass spectrometry (ICP-MS)

Immediately after the final MR session, rabbits were anesthetized and perfused transcardially with 1000 mL of cold saline. After excising the brain, 8 mm^3 regions of interest were dissected from the somatosensory cortex (AP: 1.5–3.5 mm, ML: 6–8 mm) and visual cortex (AP: 8–10 mm posterior to bregma, ML: 8–10 mm) and stored in a −80 °C freezer until processed.

Quantification of Mn^{2+} was accomplished using ICP-MS of acid digested samples. Specifically, tissue samples from left and right hemispheres were transferred to metal-free 15 mL conical tubes followed by addition of 200 μL of BDH Aristar Plus Nitric Acid (69%,VWR Scientific, Radnor, PA, USA) and incubated at 80 °C for 24 h to allow for complete sample digestion. Following digestion, ultra-pure H_2O (18.2 M Ω cm) and multi-element internal standard containing Bi, Ho, In, ^{6}Li, Sc, Tb, and Y (CLISS-1, Spex Certiprep, Metuchen, NJ, USA) were added to produce a final solution of 6.6% nitric acid (v/v) and 1 ng/mL internal standard in a total sample volume of 3 mL. Individual Mn^{2+} elemental standards were prepared by diluting a 1002 μg/mL certified Pt standard (Inorganic Ventures, Christiansburg, VA, USA) to 0.390625, 0.78125, 1.5625, 3.125, 6.25, 12.5, 25, 50, and 100 ng/g concentrations with 6.6% nitric acid (v/v), and 1 ng/mL internal standard up to a total sample volume of 5 mL.

ICP-MS was performed on a computer-controlled (QTEGRA software v.2.4) Thermo iCapQc ICP-MS (Thermo Fisher Scientific, Waltham, MA, USA) operating in standard mode and equipped with a CETAC 260 autosampler (Omaha, NE, USA), a peltier-cooled cyclonic spray chamber, and PFA self-aspirating nebuliser. Each sample was acquired using a 30 s uptake and 90 s washout time (rinse was 4% HNO_3 (v/v)), 1 survey run (3 sweeps, 5 ms dwell time) and 3 main (peak jumping) runs (100 sweeps, 10 ms dwell time). The isotopes selected for analysis were ^{55}Mn, ^{45}Sc, ^{89}Y and ^{115}In (chosen as internal standards for data interpolation). Instrument performance is optimized daily through autotuning followed by verification via a performance report (passing manufacturer specifications).

ICP-MS data for the somatosensory cortex was analyzed with the nonparametric 1-tailed Wilcoxon signed-rank test and the visual cortex was analyzed with a 2-tailed Wilcoxon signed-rank test with a p-value of <.05.

Results

Choice of Mn^{2+} dosage

Global T_1 signal intensity in the 25 mg/kg cohort increased by ~20% after two days and ~25% in the 50 mg/kg cohort demonstrating that a sufficient amount of Mn^{2+} passes the BBB and is available for accumulation in neurons (data not shown). Rabbits receiving fractionated, 5 mg/kg doses of $MnCl_2$ over ten days showed a much slower, gradual increase across time (~25% after the tenth and final dosing day). The fractionated dosing schedule was not continued due to insufficient signal enhancement on a day-to-day basis as AIM-MRI studies are contingent on having sufficient Mn^{2+} present in the extracellular space in order to accumulate within neurons.

Author Manuscript Author Manuscript Author Manuscript Author Manuscript

The decision to use 25 mg/kg Mn^{2+} for AIM-MRI experiments was also dictated by the number of complications that developed among the other groups. The rabbit receiving 100 mg/kg via the marginal ear vein developed cardiotoxicity shortly after the 3 min infusion which has been described previously (Wolf and Baum, 1983). One of the four rabbits receiving fractionated 5 mg/kg doses developed severe centribular congestion and necrosis of the liver and severe acute myocardial necrosis of the heart after 6 dose days. Finally, one rabbit receiving 50 mg/kg developed prominent lobules of the liver and hemorrhaging of the kidneys two days after the injection. Similar to previous studies reporting elevated liver enzymes after Mn^{2+} administration (Bertin et al., 2010; Thuen et al., 2008), blood work revealed significant alteration of liver enzymes alanine aminotransferase, aspartate aminotransferase, albumin, and bilirubin as well as creatine kinase in the 50 mg/kg cohort with acceptable changes in the 25 mg/kg cohort. Taken together, a dose of 25 mg/kg was determined to be sufficient to see expected signal intensity enhancement in somatosensory cortex during whisker vibration without adverse side effects.

BOLD fMRI results

In each of the three sessions, significant BOLD activation was detected in the left somatosensory (SS) cortex and left ventral posteromedial (VPM) nucleus of the thalamus (which shares reciprocal projections with the somatosensory cortex) during 60 Hz vibration of the right whiskers (Figs. 2A, C and Table 1 for percent BOLD activation values). BOLD activation demonstrated a normal block shape time course with peak amplitude approximately 10–12.5 s after whisker vibration onset (Fig. 2D, representative time course from 2nd session (6–9 h post-injection) shown). Additionally, the left SS cortex and VPM thalamus showed significant differences compared to their contralateral counterparts (Fig. 2C). Importantly, the right SS cortex, right VPM thalamus and bilateral visual cortex did not show any significant activation compared to the baseline period (Figs. 2B, C, and Table 1).

The left SS cortex and VPM thalamus demonstrated a significant time-dependent increase in BOLD activation in that subsequent sessions showed greater BOLD activation to whisker vibration (SS cortex; $F = 7.281$; $df = 2,18$; $p < .02$; VPM thalamus; $F = 11.324$; $df = 2,18$; $p < .01$). Also, the left VPM thalamus demonstrated significantly greater BOLD activation compared to the SS cortex when collapsing across sessions ($F=11.130$; $df = 1,18$; $p < .01$). Significant activation within the SS cortex comprised a greater number of voxels compared to the VPM thalamus due to a larger whisker representation in the cortex (80 vs. 17 voxels, respectively).

AIM-MRI results

Despite not disrupting the BBB, a temporal sequence of images depicting the same slice from a representative rabbit shows the effects of Mn^{2+} contrast agent accumulation (i.e. clear brightening of the image as a function of time); first, in the cerebrospinal fluid (CSF) and later in subcortical areas (Fig. 3). Time courses from the whole brain and CSF show that subcutaneous injection of Mn^{2+} into the lumbar region altered the normalized T_1W signal intensity (nSI) time courses across time (Fig. 4). In the CSF, statistical analysis revealed a significant difference among all three sessions ($F = 40.73$; $df = 2,18$; $p < .001$). nSI increased 3% over the 3 h post-injection (Fig. 4). Six to nine hours after injection, the T_1W

Author Manuscript Author Manuscript Author Manuscript Author Manuscript

nSI of the CSF was significantly enhanced compared to the first 3 h (7.4% vs. 1.2, respectively; F = 64.50; df = 1,18; p < .001) and by 24 to 27 h after $MnCl_2$ injection, the average nSI within the CSF had increased (but not significantly) to 8.8% above baseline.

There is a slight decrease in the whole brain relative to the first scan due to normalization to the pituitary gland (Pit). Because the Pit does not have a BBB, the Pit SI increases relative to the whole brain SI during the first session. However by the end of the first session and in subsequent sessions, the whole brain normalized signal intensity increases as Mn^{2+} passes the blood–CSF barrier and begins to accumulate in active neural regions.

Normalized signal intensities from the SS cortex exhibited a significant session by hemisphere interaction (F = 6.91; df = 2,18; p < .006) as shown in Fig. 5A. The nSI did not significantly differ between hemispheres by 3 h after the injection. However 6 to 9 h after injection, the nSI of the left SS cortex was significantly enhanced compared to the right SS cortex (7.5% vs. 5.0%, respectively; F = 14.01; df = 1,9; p < .005). From 24 to 27 h post-injection, the hemispheric differentiation became more pronounced in that the average nSI of the left SS cortex was enhanced 20.8% compared to a 16.4% enhancement in the right SS cortex (F = 14.83; df = 1,9; p < .004). Fig. 5C illustrates the enhancement in left relative to right somatosensory cortex nSI after the third and final session.

Normalized signal intensities from the VPM nucleus of the thalamus also exhibited a significant session by hemisphere interaction (F = 11.30; df = 2,18; p < .001) as shown in Fig. 5B. The nSI also did not significantly differ between hemispheres by 3 h after injection. Different than the SS cortex, the nSI of the VPM thalamus did not show any hemispheric differences 6–9 h post injection although the signal was significantly elevated by 6.5% compared to 0–3 h post injection (F = 282.65; df = 1,9; p < .001). By 24–27 h after injection, the nSI in the left VPM thalamus was significantly enhanced compared to the right VPM thalamus (19.2% vs. 16.0%, respectively; F = 13.57; df = 1,9; p < .005). Fig. 5C illustrates the enhancement in left relative to right VPM thalamus nSI after the third and final session.

To validate that the hemispheric T_1W differences in the somatosensory cortex and VPM thalamus were related to activity-induced Mn^{2+} accumulation and not scanner-related artifacts or preferential accumulation in the left hemisphere as a whole, the visual cortex was examined as a non-activity dependent control region. No interaction was detected between each hemisphere and the three sessions in the visual cortex as shown in Fig. 6. The nSI of the left and right visual cortex never differentiated during any of the three sessions. This confirms our assumption that the left and right hemispheres of the visual cortex show similar nSI increases presumably due to equivalent accumulation of Mn^{2+} since no differential visual stimulation was applied during the course of the experiments.

ICP-MS results

The levels of Mn^{2+} as determined by ICP-MS demonstrated a trend towards greater Mn^{2+} in the left somatosensory cortex compared to the right hemisphere, but did not reach statistical significance according to a Wilcoxon signed-rank test (1.434 vs. 1.221 μg Mn^{2+}/g tissue, respectively, Z = −1.5272, p = .076). In the visual cortex, no significance was detected between the left and right hemispheres (1.301 vs. 1.377 μg Mn^{2+}/g tissue, respectively).

Author Manuscript Author Manuscript Author Manuscript Author Manuscript

Discussion

We have demonstrated that Mn^{2+} can be administered safely and in sufficient quantity to rabbits via subcutaneous injection to achieve activity-dependent MR contrast effects in the brain. This was achieved without the need for mannitol to increase passage across the blood–brain barrier. Concurrently run BOLD fMRI experiments in the awake and conscious rabbit eliminated the bias associated with physiological effects of anesthesia on BOLD hemodynamic experiments and demonstrated BOLD activation that overlapped the Mn^{2+} signal. Our results indicate that the optimal temporal window during which subcutaneously injected Mn^{2+} is available to enter active neurons is sometime between 6 and 24 h after injection. This agrees with the mechanisms of entry into the brain after a systemic injection (Aoki et al., 2004).

While the left somatosensory (SS) cortex and left VPM thalamus showed significant unilateral BOLD activity in response to whisker vibration during each session, the SS cortex did not show differential hemispheric T_1W-associated enhancement until 6–9 h post-injection and the VPM thalamus until 24–27 h post-injection. This is likely due to insufficient Mn^{2+} being available during the 1st session for uptake to occur in these regions. Because this study did not use mannitol, Mn^{2+} enters the brain gradually over the duration of our 24 h experimental protocol. At the beginning of subsequent sessions, an elevation in nSI can be seen in all regions and some of this elevation is due to non-specific accumulation (i.e., accumulation not related to stimulation since no specific stimuli are given during the intersession period). Neurons continue to be active during this period and therefore, accumulate Mn^{2+} that is nearby. However even at the first timepoint of the 2nd session, the left SS cortex shows differential T_1W-associated enhancement. We propose that while the rabbits are in their home cage between sessions, there is preferential reverberation of the left somatosensory circuit compared to its contralateral counterpart. As a result, the left somatosensory cortex demonstrates elevated Mn^{2+} accumulation at the start of the 2nd session. This mechanism of neural reactivation after stimulation has strong support in the literature. In macaques, significant reactivation of somatosensory cortex neural ensemble activity was observed after a sequential reaching behavior (Hoffman and McNaughton, 2002). Also, repeated tactile stimulation in rats evokes unique sequential patterns of neural firing in the somatosensory cortex that reoccur during subsequent spontaneous activity (Bermudez Contreras et al., 2013). By comparing the left and right hemispheres of the SS cortex and VPM thalamus, we delineated specific and nonspecific accumulation of Mn^{2+}.

A similar mechanism applies to the left VPM thalamus, but significantly elevated Mn^{2+} accumulation is not observed until the start of the 3rd session. The reason for this delayed accumulation in the VPM thalamus is presumably due to the location of the VPM thalamus being further away from the CSF. Without BBB disruption, a spatial and temporal gradient exists for Mn^{2+} to cross into the CSF and ventricles before dispersing into the surrounding tissue leading to an ideal or preferential time window in which experimental manipulations should occur. If enough time has not elapsed, too little Mn^{2+}would be available in the extracellular space for cells to accumulate Mn^{2+} whereas waiting too long before experiments are performed would allow Mn^{2+} to accumulate nonspecifically and become sequestered. For regions farther away from the CSF and ventricles, extra time may be

Author Manuscript Author Manuscript Author Manuscript Author Manuscript

needed for enough Mn^{2+} to be accessible to the active neurons subserving the functional activity. The VPM thalamus, which is situated farther away from the CSF compared to the SS cortex, begins to show differential nSI between hemispheres 24 h post-injection presumably due to Mn^{2+} being available for uptake.

It is worth noting that by 6–9 h post-injection, the nSI enhancement in the CSF appears to stabilize. This would suggest that there exists a steady state in which Mn^{2+} is being absorbed into the bloodstream, entering the choroid plexus, CSF and ventricles within 2 h before seeping into the surrounding extracellular space (Aoki et al., 2004). Additionally it appears that by 24 h post-injection, the nSI of SS cortex, VPM thalamus, and visual cortical areas reach a similar plateau given that the effect of time within session for each region was not significant during the 24–27 h session.

BOLD activation increased across sessions in the left SS cortex and VPM thalamus presumably as a result of repeated stimulation. Previous studies have also observed stimulus-related increases in somatosensory pathway activity. In the rat barrel cortex in which only two whiskers are left intact, a significant increase in response is seen 3.5 days later compared to rats whose whiskers were left intact (Lebedev et al., 2000). Also, using whisker vibration as a conditioned stimulus in trace eyeblink conditioning leads to learning-specific metabolic activity increases in the whisker-barrel somatosensory cortex as measured with cytochrome oxidase staining (Galvez et al., 2006).

The lack of a significant difference in Mn^{2+} content as measured by ICP-MS in extracted tissue could be explained by the relatively large piece (8 mm^3) cut from each hemisphere. While the spatial locations are similar for the significant BOLD activation in the left somatosensory cortex and that of our excised regions, smaller, more precisely located, tissue volumes may be necessary to demonstrate a hemispheric difference in Mn^{2+} content.

Mn^{2+} dose-dependent toxicology

In order to fully exploit AIM-MRI for cognitive studies, it is important to determine several operational parameters, including physiological parameters which determine Mn^{2+} biodistribution and pharmacokinetics, dosage, mode of administration and timing and length of experimental manipulations (i.e. timing of stimuli following injection of $MnCl_2$). Our pilot study examining a series of dosages and administrations indicated that an injection of 25 mg/kg provided sufficient T_1W signal enhancement without the need to open the blood–brain barrier and without adverse effects on liver function.

Conclusions

This is the first examination of AIM-MRI concurrently with BOLD imaging in an awake and conscious rabbit in order to co-localize changes in T_1W signal intensity as a result of Mn^{2+} accumulation. Consequently, our results are not biased by any physiological alteration of neural activation caused by anesthesia or sedation. Additionally, the experiments described in this work demonstrate that subcutaneous administration of Mn^{2+} at a sufficient dosage for AIM-MRI and with minimal toxic effects allows relatively slow but constant biodistribution kinetics which are well suited for neuronal uptake in the awake rabbit. With

Author Manuscript Author Manuscript Author Manuscript Author Manuscript

AIM-MRI studies, experimental manipulations and subsequent MR imaging can be timed to acquire a “snapshot” of the active regions showing significant accumulation of Mn^{2+} just prior to euthanasia so that Mn^{2+} toxicity can be minimized.

Acknowledgments

This work was supported by the National Institutes of Health (National Institute of Neurological Disorders and Stroke Grant NS059879 and the National Institute of Mental Health Grant MH47340). M.S. was supported by the T32 Training Program: The Neuroscience of Human Cognition at Northwestern University (T32-NS047987).

Metal analysis was performed at the Northwestern University Quantitative Bioelemental Imaging Center generously supported by NASA Ames Research Center Grant NNA04CC36G.

References

Aoki I, Tanaka C, Takegami T, Ebisu T, Umeda M, Fukunaga M, Fukuda K, Silva AC, Koretsky AP, Naruse S. Dynamic activity-induced manganese-dependent contrast magnetic resonance imaging (DAIM MRI). Magn. Reson. Med. 2002; 48:927–933. http://dx.doi.org/10.1002/mrm.10320. [PubMed: 12465100]

Aoki I, Wu Y-JL, Silva AC, Lynch RM, Koretsky AP. In vivo detection of neuroarchitecture in the rodent brain using manganese-enhanced MRI. NeuroImage. 2004; 22:1046–1059. http://dx.doi.org/10.1016/j.neuroimage.2004.03.031. [PubMed: 15219577]

Berkowitz BA, Roberts R, Goebel DJ, Luan H. Noninvasive and simultaneous imaging of layer-specific retinal functional adaptation by manganese-enhanced MRI. Invest. Ophthalmol. Vis. Sci. 2006; 47:2668–2674. http://dx.doi.org/10.1167/iovs.05-1588. [PubMed: 16723485]

Bermudez Contreras EJ, Schjetnan AGP, Muhammad A, Bartho P, McNaughton BL, Kolb B, Gruber AJ, Luczak A. Formation and reverberation of sequential neural activity patterns evoked by sensory stimulation are enhanced during cortical desynchronization. Neuron. 2013; 79:555–566. http://dx.doi.org/10.1016/j.neuron.2013.06.013. [PubMed: 23932001]

Bertin A, Michou-Gallani A-I, Gallani J-L, Felder-Flesch D. In vitro neurotoxicity of magnetic resonance imaging (MRI) contrast agents: influence of the molecular structure and paramagnetic ion. Toxicol. In Vitro. 2010; 24:1386–1394. http://dx.doi.org/10.1016/j.tiv.2010.05.001. [PubMed: 20460148]

Bissig D, Berkowitz BA. Manganese-enhanced MRI of layer-specific activity in the visual cortex from awake and free-moving rats. NeuroImage. 2009; 44:627–635. http://dx.doi.org/10.1016/j.neuroimage.2008.10.013. [PubMed: 19015035]

Bock NA, Paiva FF, Nascimento GC, Newman JD, Silva AC. Cerebro-spinal fluid to brain transport of manganese in a non-human primate revealed by MRI. Brain Res. 2008a; 1198:160–170. http://dx.doi.org/10.1016/j.brainres.2007.12.065. [PubMed: 18243167]

Bock NA, Paiva FF, Silva AC. Fractionated manganese-enhanced MRI. NMR Biomed. 2008b; 21:473–478. http://dx.doi.org/10.1002/nbm.1211. [PubMed: 17944008]

Bornhorst J, Wehe CA, Hüwel S, Karst U, Galla H-J, Schwerdtle T. Impact of manganese on and transfer across blood–brain and blood–cerebrospinal fluid barrier in vitro. J. Biol. Chem. 2012; 287:17140–17151. http://dx.doi.org/10.1074/jbc.M112.344093. [PubMed: 22457347]

Brevard ME, Duong TQ, King JA, Ferris CF. Changes in MRI signal intensity during hypercapnic challenge under conscious and anesthetized conditions. Magn. Reson. Imaging. 2003; 21:995–1001. [PubMed: 14684202]

Cacace AT, Brozoski T, Berkowitz B, Bauer C, Odintsov B, Bergkvist M, Castracane J, Zhang J, Holt AG. Manganese enhanced magnetic resonance imaging (MEMRI): a powerful new imaging method to study tinnitus. Hear. Res. 2014; 311:49–62. http://dx.doi.org/10.1016/j.heares.2014.02.003. [PubMed: 24583078]

Chandra SV, Shukla GS. Role of iron deficiency in inducing susceptibility to manganese toxicity. Arch. Toxicol. 1976; 35:319–323. [PubMed: 989299]

Author Manuscript Author Manuscript Author Manuscript Author Manuscript

Chuang K-H, Koretsky AP. Accounting for nonspecific enhancement in neuronal tract tracing using manganese enhanced magnetic resonance imaging. Magn. Reson. Imaging. 2009; 27:594–600. http://dx.doi.org/10.1016/j.mri.2008.10.006. [PubMed: 19144489]

Chuang K-H, Koretsky AP, Sotak CH. Temporal changes in the T1 and T2 relaxation rates (DeltaR1 and DeltaR2) in the rat brain are consistent with the tissue-clearance rates of elemental manganese. Magn. Reson. Med. 2009; 61:1528–1532. http://dx.doi.org/10.1002/mrm.21962. [PubMed: 19353652]

Couture P, Hulbert AJ. Relationship between body mass, tissue metabolic rate, and sodium pump activity in mammalian liver and kidney. Am. J. Physiol. 1995; 268:R641–R650. [PubMed: 7900906]

Cox RW. AFNI: software for analysis and visualization of functional magnetic resonance neuroimages. Comput. Biomed. Res. 1996; 29:162–173. [PubMed: 8812068]

Crossgrove J, Zheng W. Manganese toxicity upon overexposure. NMR Biomed. 2004; 17:544–553. http://dx.doi.org/10.1002/nbm.931. [PubMed: 15617053]

Das S, Weiss C, Disterhoft JF. Eyeblink conditioning in the rabbit (*Oryctolagus cuniculus*) with stimulation of the mystacial vibrissae as a conditioned stimulus. Behav. Neurosci. 2001; 115:731–736. [PubMed: 11439462]

Dobson GP, Headrick JP. Bioenergetic scaling: metabolic design and body-size constraints in mammals. Proc. Natl. Acad. Sci. U. S. A. 1995; 92:7317–7321. [PubMed: 7638188]

Drapeau P, Nachshen DA. Manganese fluxes and manganese-dependent neurotransmitter release in presynaptic nerve endings isolated from rat brain. J. Physiol. 1984; 348:493–510. [PubMed: 6325673]

Eschenko O, Canals S, Simanova I, Beyerlein M, Murayama Y, Logothetis NK. Mapping of functional brain activity in freely behaving rats during voluntary running using manganese-enhanced MRI: implication for longitudinal studies. NeuroImage. 2010; 49:2544–2555. http://dx.doi.org/10.1016/j.neuroimage.2009.10.079. [PubMed: 19896539]

Furchner JE, Richmond CR, Drake GA. Comparative metabolism of radionuclides in mammals. 3. Retention of manganese-54 in the mouse, rat, monkey and dog. Health Phys. 1966; 12:1415–1423. [PubMed: 4961684]

Galvez R, Weiss C, Weible AP, Disterhoft JF. Vibrissa-signaled eyeblink conditioning induces somatosensory cortical plasticity. J. Neurosci. 2006; 26:6062–6068. http://dx.doi.org/10.1523/JNEUROSCI.5582-05.2006. [PubMed: 16738249]

Hoffman KL, McNaughton BL. Coordinated reactivation of distributed memory traces in primate neocortex. Science. 2002; 297:2070–2073. http://dx.doi.org/10.1126/science.1073538. [PubMed: 12242447]

Inoue T, Majid T, Pautler RG. Manganese enhanced MRI (MEMRI): neurophysiological applications. Rev. Neurosci. 2011; 22:675–694. http://dx.doi.org/10.1515/RNS.2011.048. [PubMed: 22098448]

Kim H, Cho J, Kim YR, Song Y, Chun S-I, Suh J-Y, Kim JK, Ryu Y-H, Choi S-M, Cho H, Cho G. Response of the primary auditory and non-auditory cortices to acoustic stimulation: a manganese-enhanced MRI study. PLoS One. 2014; 9:e90427. http://dx.doi.org/10.1371/journal.pone.0090427. [PubMed: 24618696]

Kuo Y-T, Herlihy AH, So P-W, Bell JD. Manganese-enhanced magnetic resonance imaging (MEMRI) without compromise of the blood–brain barrier detects hypothalamic neuronal activity in vivo. NMR Biomed. 2006; 19:1028–1034. http://dx.doi.org/10.1002/nbm.1070. [PubMed: 16845705]

Kuo Y-T, Parkinson JRC, Chaudhri OB, Herlihy AH, So P-W, Dhillo WS, Small CJ, Bloom SR, Bell JD. The temporal sequence of gut peptide CNS interactions tracked in vivo by magnetic resonance imaging. J. Neurosci. 2007; 27:12341–12348. http://dx.doi.org/10.1523/JNEUROSCI.2391-07.2007. [PubMed: 17989298]

Lebedev MA, Mirabella G, Erchova I, Diamond ME. Experience-dependent plasticity of rat barrel cortex: redistribution of activity across barrel-columns. Cereb. Cortex. 2000; 10:23–31. [PubMed: 10639392]

Lee JH, Durand R, Gradinaru V, Zhang F, Goshen I, Kim D-S, Fenno LE, Ramakrishnan C, Deisseroth K. Global and local fMRI signals driven by neurons defined optogenetically by type

Author Manuscript Author Manuscript Author Manuscript Author Manuscript

and wiring. Nature. 2010; 465:788–792. http://dx.doi.org/10.1038/nature09108. [PubMed: 20473285]

Lev-Tov A, O'Donovan MJ. Calcium imaging of motoneuron activity in the en-bloc spinal cord preparation of the neonatal rat. J. Neurophysiol. 1995; 74:1324–1334. [PubMed: 7500153]

Li L, Weiss C, Talk AC, Disterhoft JF, Wyrwicz AM. A MRI-compatible system for whisker stimulation. J. Neurosci. Methods. 2012; 205:305–311. http://dx.doi.org/10.1016/j.jneumeth.2012.01.014. [PubMed: 22322316]

Lin YJ, Koretsky AP. Manganese ion enhances T1-weighted MRI during brain activation: an approach to direct imaging of brain function. Magn. Reson. Med. 1997; 38:378–388. [PubMed: 9339438]

Liu X, Zhu X-H, Zhang Y, Chen W. The change of functional connectivity specificity in rats under various anesthesia levels and its neural origin. Brain Topogr. 2013; 26:363–377. http://dx.doi.org/10.1007/s10548-012-0267-5. [PubMed: 23208517]

Logothetis NK, Pauls J, Augath M, Trinath T, Oeltermann A. Neurophysiological investigation of the basis of the fMRI signal. Nature. 2001; 412:150–157. http://dx.doi.org/10.1038/35084005. [PubMed: 11449264]

McClellan AD, McPherson D, O'Donovan MJ. Combined retrograde labeling and calcium imaging in spinal cord and brainstem neurons of the lamprey. Brain Res. 1994; 663:61–68. [PubMed: 7531597]

Narita K, Kawasaki F, Kita H. Mn and Mg influxes through Ca channels of motor nerve terminals are prevented by verapamil in frogs. Brain Res. 1990; 510:289–295. http://dx.doi.org/10.1016/0006-8993(90)91379-U. [PubMed: 2158851]

Pautler RG, Silva AC, Koretsky AP. In vivo neuronal tract tracing using manganese-enhanced magnetic resonance imaging. Magn. Reson. Med. 1998; 40:740–748. [PubMed: 9797158]

Porter RK, Brand MD. Cellular oxygen consumption depends on body mass. Am. J. Physiol. 1995; 269:R226–R228. [PubMed: 7631898]

Regehr W, Tank D. Calcium concentration dynamics produced by synaptic activation of CA1 hippocampal pyramidal cells. J. Neurosci. 1992; 12:4202–4223. [PubMed: 1359030]

Schmitt C, Strazielle N, Richaud P, Bouron A, Ghersi-Egea J-F. Active transport at the blood–CSF barrier contributes to manganese influx into the brain. J. Neurochem. 2011; 117:747–756. http://dx.doi.org/10.1111/j.1471-4159.2011.07246.x. [PubMed: 21395586]

Seo Y, Satoh K, Watanabe K, Morita H, Takamata A, Ogino T, Murakami M. Mn-bicine: a low affinity chelate for manganese ion enhanced MRI. Magn. Reson. Med. 2011; 65:1005–1012. http://dx.doi.org/10.1002/mrm.22680. [PubMed: 21413064]

Sepúlveda MR, Dresselaers T, Vangheluwe P, Everaerts W, Himmelreich U, Mata AM, Wuytack F. Evaluation of manganese uptake and toxicity in mouse brain during continuous MnCl(2) administration using osmotic pumps. Contrast Media Mol. Imaging. 2012; 7:426–434. http://dx.doi.org/10.1002/cmmi.1469. [PubMed: 22649049]

Shazeeb MS, Sotak CH. Dose dependence and temporal evolution of the T1 relaxation time and MRI contrast in the rat brain after subcutaneous injection of manganese chloride. Magn. Reson. Med. 2012; 68:1955–1962. http://dx.doi.org/10.1002/mrm.24184. [PubMed: 22294279]

Silva AC. Using manganese-enhanced MRI to understand BOLD. NeuroImage. 2012; 62:1009–1013. http://dx.doi.org/10.1016/j.neuroimage.2012.01.008. [PubMed: 22245640]

Silva AC, Bock NA. Manganese-enhanced MRI: an exceptional tool in translational neuroimaging. Schizophr. Bull. 2008; 34:595–604. http://dx.doi.org/10.1093/schbul/sbn056. [PubMed: 18550591]

Silva AC, Lee JH, Aoki I, Koretsky AP. Manganese-enhanced magnetic resonance imaging (MEMRI): methodological and practical considerations. NMR Biomed. 2004; 17:532–543. http://dx.doi.org/10.1002/nbm.945. [PubMed: 15617052]

Sloot WN, Gramsbergen JB. Axonal transport of manganese and its relevance to selective neurotoxicity in the rat basal ganglia. Brain Res. 1994; 657:124–132. [PubMed: 7820609]

Takeda A, Kodama Y, Ishiwatari S, Okada S. Manganese transport in the neural circuit of rat CNS. Brain Res. Bull. 1998; 45:149–152. [PubMed: 9443831]

Thuen M, Berry M, Pedersen TB, Goa PE, Summerfield M, Haraldseth O, Sandvig A, Brekken C. Manganese-enhanced MRI of the rat visual pathway: acute neural toxicity, contrast enhancement,

Author Manuscript Author Manuscript Author Manuscript Author Manuscript

axon resolution, axonal transport, and clearance of Mn(2+). J. Magn. Reson. Imaging. 2008; 28:855–865. http://dx.doi.org/10.1002/jmri.21504. [PubMed: 18821627]

Tjälve H, Mejàre C, Borg-Neczak K. Uptake and transport of manganese in primary and secondary olfactory neurones in pike. Pharmacol. Toxicol. 1995; 77:23–31. [PubMed: 8532608]

Watanabe T, Radulovic J, Spiess J, Natt O, Boretius S, Frahm J, Michaelis T. In vivo 3D MRI staining of the mouse hippocampal system using intracerebral injection of MnCl2. NeuroImage. 2004; 22:860–867. http://dx.doi.org/10.1016/j.neuroimage.2004.01.028. [PubMed: 15193616]

Watanabe T, Frahm J, Michaelis T. Manganese-enhanced MRI of the mouse auditory pathway. Magn. Reson. Med. 2008; 60:210–212. http://dx.doi.org/10.1002/mrm.21645. [PubMed: 18581385]

Watanabe T, Frahm J, Michaelis T. Reduced intracellular mobility underlies manganese relaxivity in mouse brain in vivo: MRI at 2.35 and 9.4 T. Brain Struct. Funct. 2014 http://dx.doi.org/10.1007/s00429-014-0742-8.

Weng J-C, Chen J-H, Yang P-F, Tseng W-YI. Functional mapping of rat barrel activation following whisker stimulation using activity-induced manganese-dependent contrast. NeuroImage. 2007; 36:1179–1188. http://dx.doi.org/10.1016/j.neuroimage.2007.04.010. [PubMed: 17537649]

Wolf GL, Baum L. Cardiovascular toxicity and tissue proton T1 response to manganese injection in the dog and rabbit. AJ. Am. J. Roentgenol. 1983; 141:193–197. http://dx.doi.org/10.2214/ajr.141.1.193.

Yoshida R, Iwamoto A, Nagahama T. Calcium imaging for detection and estimation of spike activities in Aplysia neurons. Zool. Sci. 2001; 18:631–643. http://dx.doi.org/10.2108/zsj.18.631.

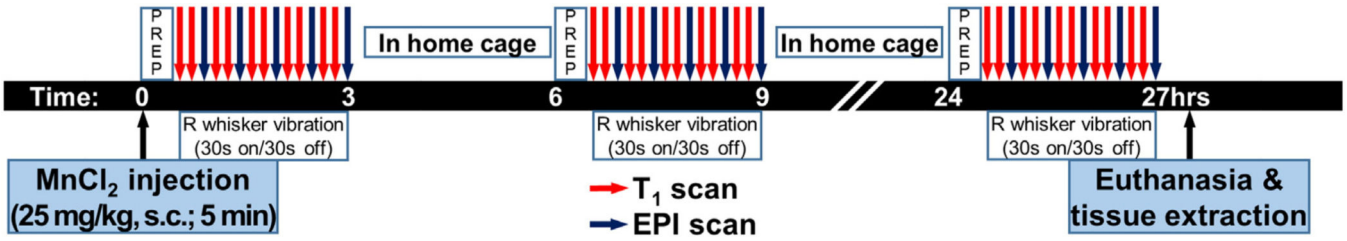

Fig. 1.
Schematic timeline of experiments (abbreviation: s.c. = subcutaneous).

Author Manuscript Author Manuscript Author Manuscript Author Manuscript

Author Manuscript
Author Manuscript
Author Manuscript
Author Manuscript

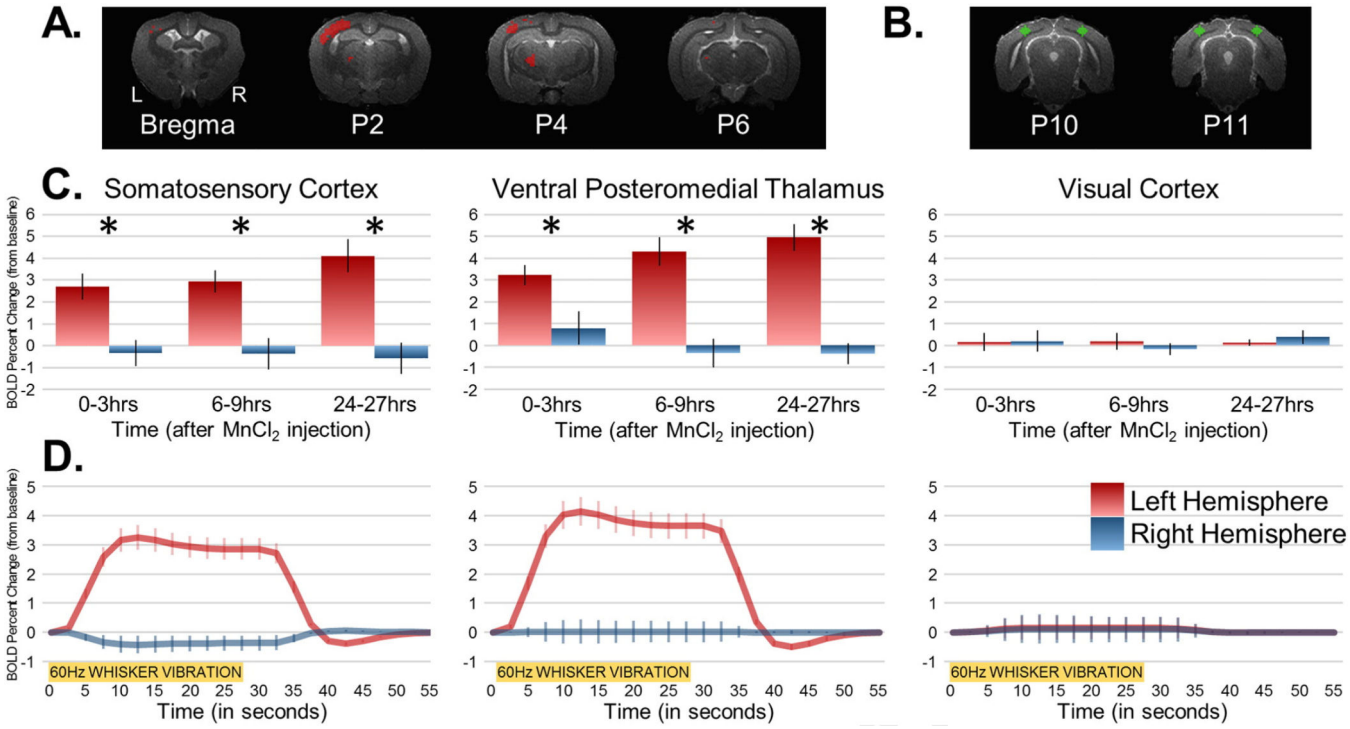

Fig. 2.

BOLD activation in response to right whisker vibration. A. Mask of significantly active voxels ($p < .001$, obtained via repeated-measures ANOVA) in the contralateral whisker-related somatosensory cortex and ventral posteromedial thalamus during 60 Hz vibration of right whiskers in rabbits ($n = 10$). B. Spatial map of visual cortex control regions of interest. C. BOLD percent signal change (mean ± SEM) in the somatosensory cortex, ventral posteromedial nucleus of the thalamus, and visual cortex. The contralateral somatosensory system has significantly greater BOLD response compared to the ipsilateral side. The visual cortex shows a minimal, non-significant BOLD response during whisker stimulation. Asterisks denote significant difference between hemispheres. D. Representative time course profiles (mean ± SEM) from the 2nd session (i.e., 6–9 h post-injection) of the three regions during whisker vibration.

Author Manuscript Author Manuscript Author Manuscript Author Manuscript

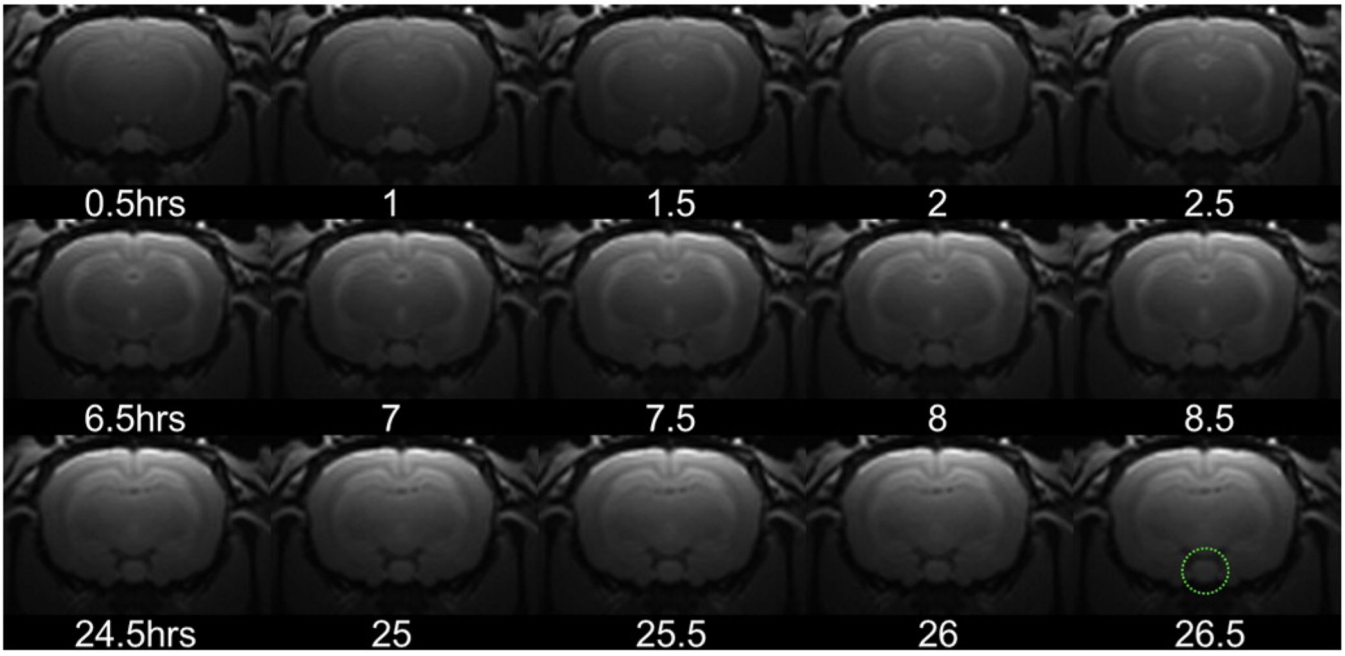

Fig. 3.

T_1-weighted (T_1W) MRI images after $MnCl_2$ injection. From a representative rabbit, brightening of the image at the specified hours is a result of Mn^{2+} accumulation producing shorter T_1 relaxation times. Pituitary gland is outlined in green in the lower right image.

Author Manuscript
Author Manuscript
Author Manuscript
Author Manuscript

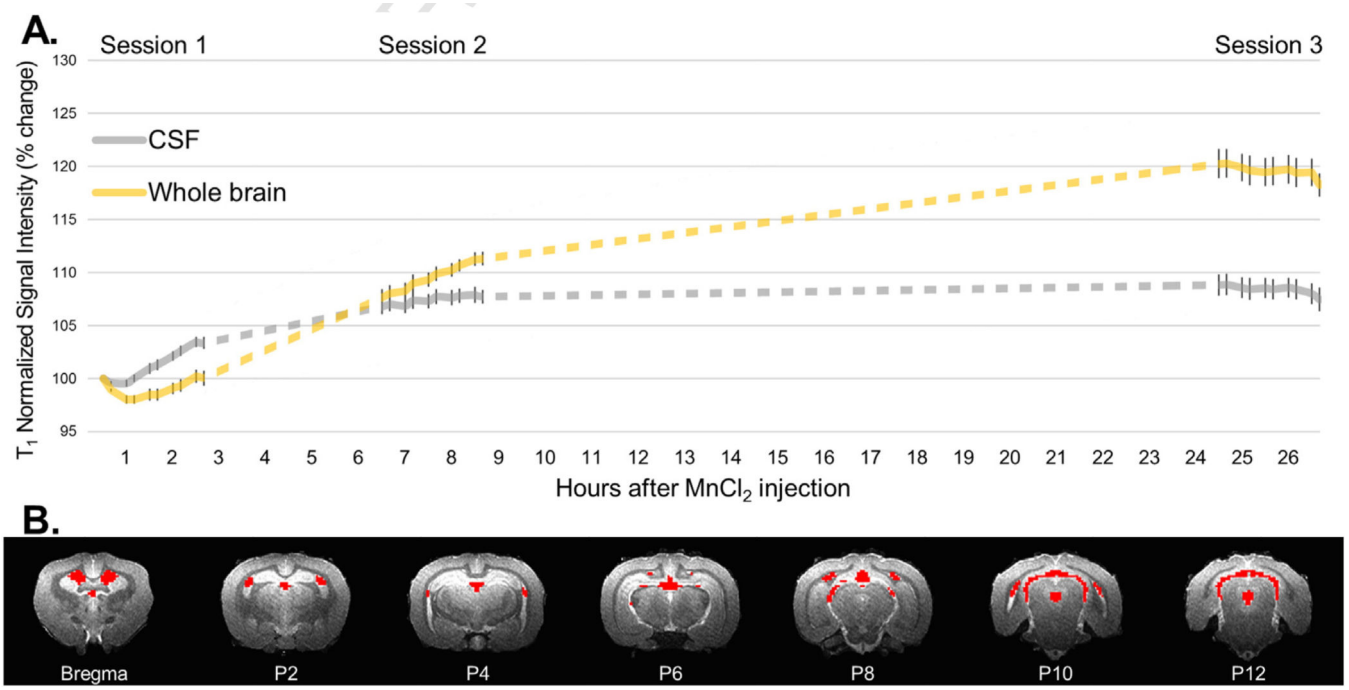

Fig. 4.

T_1W signal intensity profiles of whole brain and CSF. A. T_1W signal intensity profile (normalized to pituitary gland and relative to first scan from first session) from cerebrospinal fluid (CSF) and whole brain (mean±SEM). Linear curve-fitting method employed. Yellow line = whole brain, gray line = CSF. Dotted lines denote time spent in home cage between sessions and is meant to provide a "guide to the eye". B. Mask of CSF voxels.

Author Manuscript Author Manuscript Author Manuscript Author Manuscript

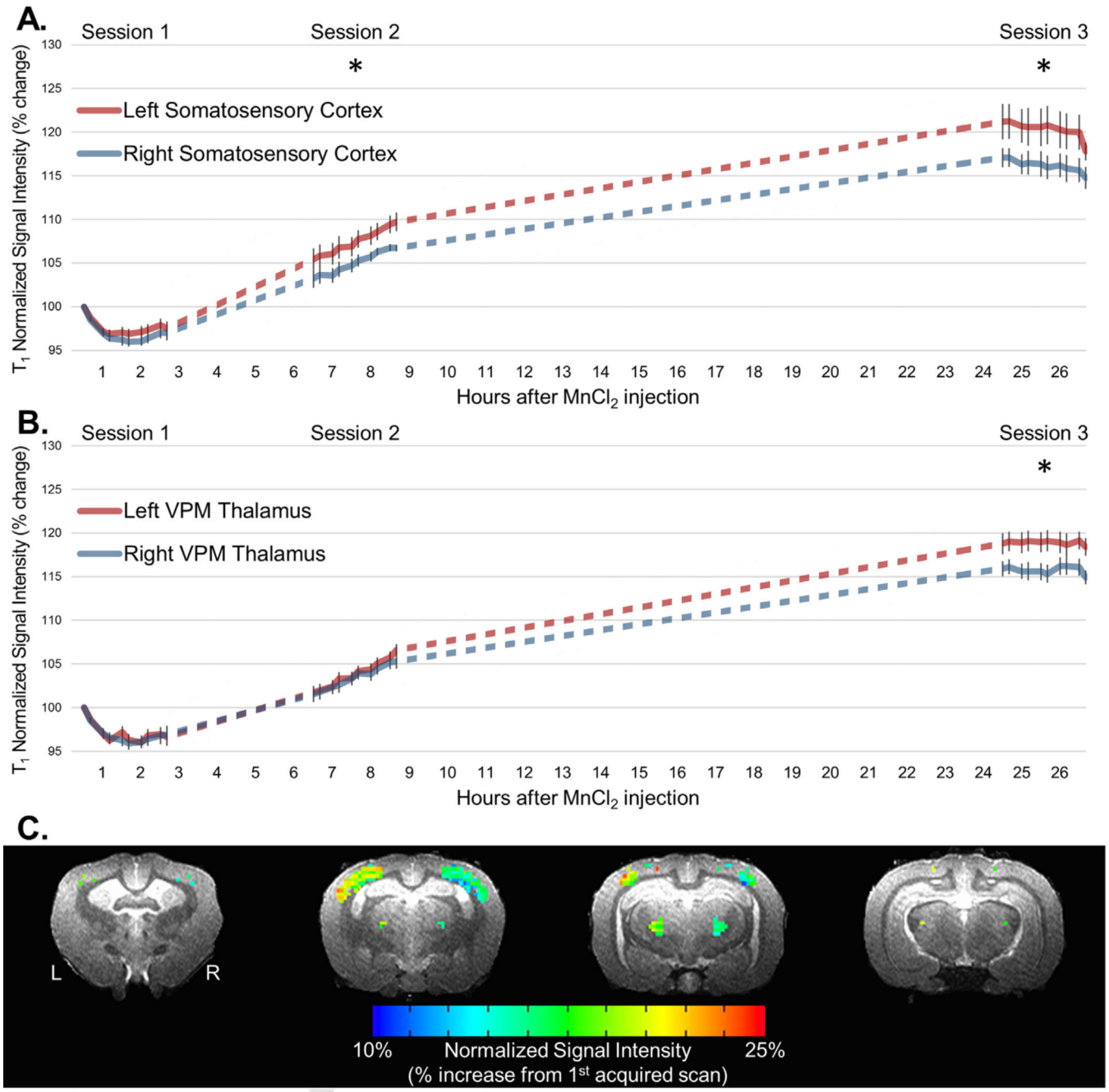

Fig. 5.

T_1W signal intensity profiles and color maps of somatosensory cortex and VPM thalamus showing significant differential Mn^{2+} accumulation. A. T_1W signal intensity profile (normalized to pituitary gland and relative to first scan from first session) from somatosensory cortex (mean ± SEM). Asterisks denote significant post-hoc hemispheric differences during 6–9 h (2nd) and 24–27 h (3rd) post-injection session ($p < .05$). Red line = left somatosensory cortex (contralateral to right whisker vibration), blue line = right somatosensory cortex (ipsilateral to right whisker vibration). Dotted lines denote time spent in home cage between sessions and is meant to provide a "guide to the eye". B. T_1W signal

Author Manuscript Author Manuscript Author Manuscript Author Manuscript

intensity profile (normalized to pituitary gland) from ventral posteromedial nucleus of the thalamus (mean ± SEM). Asterisk denotes significant post-hoc hemispheric differences during 24–27 h (3rd) post-injection session ($p < .05$). Red line = left VPM thalamus (contralateral to right whisker vibration), blue line = Right VPM thalamus (ipsilateral to right whisker vibration). Linear curve-fitting method employed. C. Color maps from the end of session 3 displaying significant accumulation on Mn^{2+} in the left somatosensory cortex and VPM thalamus relative to right hemisphere.

Author Manuscript Author Manuscript Author Manuscript Author Manuscript

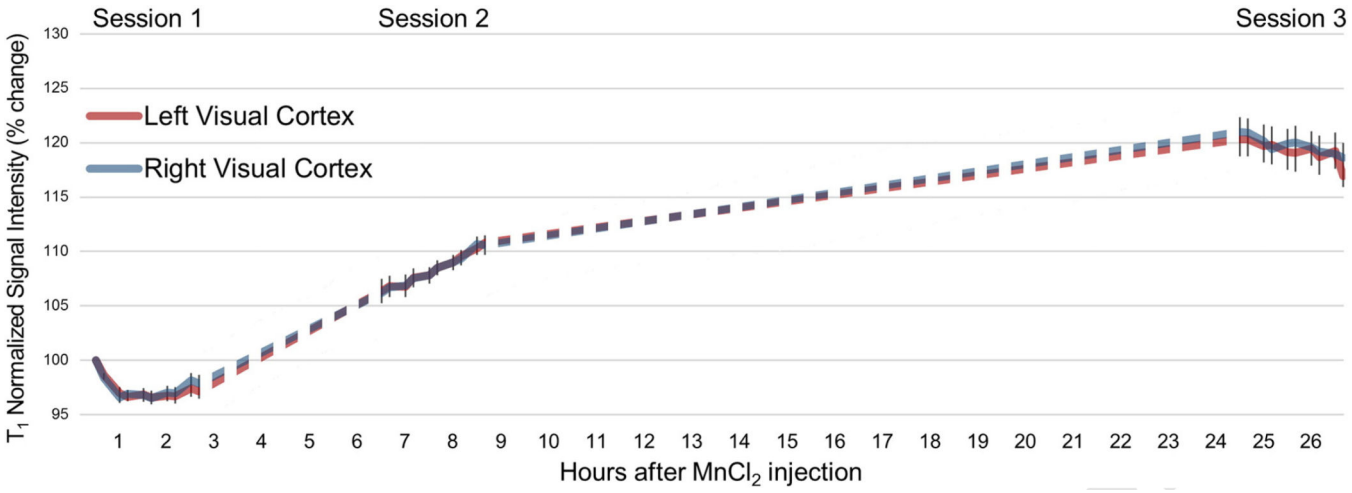

Fig. 6.

Hemispheres of visual cortex do not differ in T_1W signal intensity profiles. T_1W normalized signal intensity profile from visual cortex (normalized to pituitary gland and relative to first scan from first session) (mean ± SEM). No significant session × hemisphere interaction and no hemispheric differences during any session ($p > .05$). Red line = left visual cortex (contralateral to right whisker vibration), blue line = right visual cortex (ipsilateral to right whisker vibration). Linear curve-fitting method employed. Dotted lines denote time spent in home cage between sessions and is meant to provide a "guide to the eye".

Author Manuscript

Author Manuscript

Author Manuscript

Author Manuscript

Table 1

BOLD activation (% change) in response to right whisker vibration. BOLD activation in the left somatosensory cortex and left VPM thalamus show a significant response to right whisker vibration. The counterparts in the right hemisphere as well as the visual cortex do not exhibit any significant BOLD activation to whisker vibration.

Region	Left hemisphere BOLD % signal change (contralateral to whisker vibration)		Mean *t* value	Right hemisphere BOLD % signal change (ipsilateral to whisker vibration)
Somatosensory cortex	0–3 h	2.70%	2.50***	−0.33%^
	6–9 h	2.95%	3.09***	−0.37%^
	24–27 h	4.16%	4.30***	−0.59%^
Ventral posteromedial thalamus	0–3 h	3.27%	2.42***	0.79%^
	6–9 h	4.31%	3.90***	−0.35%^
	24–27 h	4.95%	4.09***	−0.38%^
Visual cortex	0–3 h	0.15%	0.61	0.19%
	6–9 h	0.19%	0.48	−0.16%
	24–27 h	0.13%	0.25	0.39%

*** Denotes significant difference compared to baseline activation ($p < .001$, df = 1,9).

^ Denotes significant difference between hemispheres ($p < .05$, df = 1,9).